




Analysis of illumination dependent electrical characteristics of α - styryl substituted BODIPY dye-based hybrid heterojunction

Nazmiye Kaplan¹, Enis Taşçı², Mustafa Emrulloğlu³, Halil Gökce², Nihat Tuğluoğlu¹, and Serkan Eymur^{1,*} 

¹Department of Energy Systems Engineering, Giresun University, Giresun, Turkey

²Vocational School of Health Services, Giresun University, Giresun, Turkey

³Department of Photonics, İzmir Institute of Technology, İzmir, Turkey

Received: 10 March 2021

Accepted: 18 May 2021

Published online:
27 May 2021

© The Author(s), under exclusive licence to Springer Science+Business Media, LLC, part of Springer Nature 2021

ABSTRACT

The α -styryl substituted BODIPY compound (BDP-Sty) was synthesized and characterized. The optimized ground state structure, HOMO and LUMO simulations, MEP surface map, and various molecular descriptors of the isolated BDP-Sty compound were investigated by Density Functional Theory at the B3LYP/6-311G (d,p) level. The reverse and forward bias current-voltage (I - V) characteristics of the Au/BDP-Sty/n-Si/In diode showed Schottky diode-like characteristics. An ideality factor (n) and barrier height (Φ_b) values of prepared diode for dark were found as 2.32 and 0.828, respectively. The series resistance (R_s) values were attained from the $dV/d\ln(I)$ plot and Cheung's $H(I)$ function and their values found for dark as 4.95 k Ω and 4.59 k Ω , respectively. The $\ln I - \ln V$ and $\ln(I_R) - V_R^{1/2}$ characteristics of the Au/BDP-Sty/n-Si/In diode reveal that the conduction mechanism is ohmic at low voltage and that of trap-filled space charge limited current and space charge limited current at higher voltage. The characteristic photodiode parameters of the prepared diode such as open circuit voltage (V_{oc}), short circuit current density (J_{sc}), and photosensitivity (S) have also been investigated. All these results indicate the applicability for Au/BDP-Sty/n-Si/In diode in the field optoelectronic device applications.

1 Introduction

Metal–semiconductor (MS) contact is one of the rectifier contacts used as a basic component in the electronic and optoelectronic applications, including transistors, capacitors and diodes [1–3]. Due to the

technological importance of MS contacts, the structural and electrical properties of metal–insulator–semiconductor and solar cells have been studied in detail for a long time. The full understanding of the nature of the electrical characteristics of Schottky diodes (SDs), one of the simplest MS contact devices,

Address correspondence to E-mail: serkan.eymur@giresun.edu.tr

is of great interest due to their technological importance. Recently, there has been a growing interest in efforts to improve the performance, reliability and quality of SDs by controlling diode parameters such as series resistance of the device and barrier height at the MS interface using an interlayer. Specially, the choice of the interfacial layer, its type, thickness and permittivity are of great importance for improving the performance and reliability of these SBDs. Namely, this modification using the interface layer or insulating layer plays an important role in junction parameters such as R_s , n , Φ_b , reverse saturation current (I_0) and density of interface states (N_{ss}), resulting in major changes in the electronics characteristics of the device. For instance, the current conduction mechanisms and electrical parameters of SDs have been controlled by using insulators, polymers or small molecule organic semiconductors as an interlayer at metal/semiconductor [4–17].

Due to the important advantages of organic semiconducting compounds such as high dielectric constant, charge storage capacity and photostability, they have become a widespread research subject for the design and construction of semiconductor-based devices [18, 19]. Among different types of organic semiconductors, organic dyes have been intensively studied over past decades, owing to their low cost, good solubility in organic solvents, high chemical stability and high photoconductive properties [11, 12, 20–24]. Especially, BODIPY (4,4-difluoro-4-bora-3a,4a-diaza-s-indacene) and its derivatives, one of the most popular fluorescent dye, have emerged as a promising candidate to obtain organic based electronic devices [25–28]. Due to its large π -conjugated structure, high extinction coefficient, narrow emission bands, it is not surprising that BODIPY derivatives have gained great importance recently in diverse applications such as chemosensors, energy-transfer cassettes and sensitizers for solar cells [25, 27, 29–34]. Among these studies, only few studies have been found in the literature on the effect of using π -conjugated BODIPY derivatives as an interfacial layer on the structural and optical properties of Au/n-Si thin film [27, 35–37]. In this context, the synthesis of BODIPY derivatives with high semiconductor level and the investigation of their effects on the main diode parameters of SDs is still an interesting subject.

Considering the importance of π -conjugated BODIPY compounds for optoelectronic devices, we have

been focused on the synthesis of α -styryl substituted BODIPY π -system (BDP-Sty) (Fig. 1). The main purpose of this study is to investigate the effect of π -conjugated BODIPY (BDP-Sty) interlayer on the electrical and photoelectrical parameters of Au/n-Si type Schottky diode. For this aim, BDP-Sty compound was synthesized according to literature. Then, molecular orbital calculations have been studied by DFT-B3LYP/6-311G(d,p) computational level to obtain various structural parameters. Finally, Au/BDP-Sty/n-Si structure have been fabricated to show the effect of BDP-Sty compound on the illumination dependent electrical and photoelectrical properties of dependent I - V characteristics of the diode.

2 Experimental

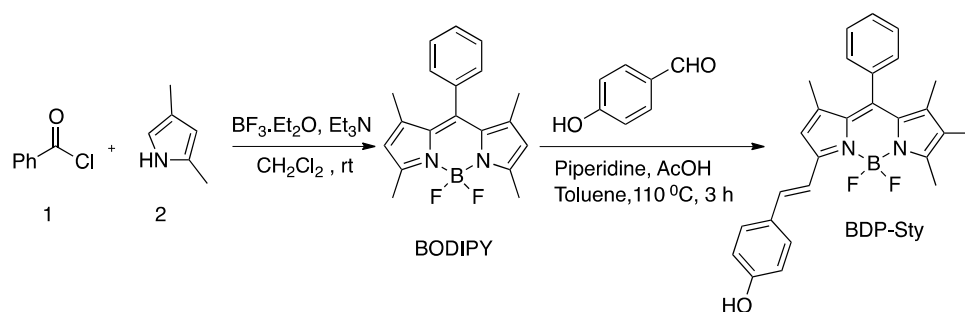
2.1 Synthetic procedure for BDP-Sty

BODIPY and BDP-Sty compounds were synthesized according to procedures published in literature [38]. Under argon atmosphere, BODIPY (400 mg, 1.23 mmol), 4-hydroxybenzaldehyde (165 mg, 1.35 mmol), 0.9 ml piperidine and 0.6 ml glacial acetic acid were taken up in toluene (30 ml) and the mixture was refluxed 3 h. Then water was added into it and crude mixture was extracted with dichloromethane. The organic layer was dried over anhydrous $MgSO_4$, filtered and concentrated under reduced pressure. The residue was subjected to column chromatography on silica gel using EtOAc:hexane (1:9) as the eluent, which gave the pure compound as red solid (yield: 48%); The identity of the BDP-Sty was unambiguously confirmed by 1H and ^{13}C spectroscopy.

2.2 Fabrication of Au/BDP-Sty/n-Si/In diode

A n-Si wafer with a (100) orientation, 500 μm thickness and 20 Ωcm resistivity was used to fabricate the Au/BDP-Sty/n-Si diode. Before making contacts, a n-type Si wafer was chemically cleaned to eliminate the impurities and inherent oxide layer on surface by using standard RCA cleaning method, *i.e.*, 10 min boil in $NH_3 + H_2O_2 + 6H_2O$ after that a 10 min HCl + $H_2O_2 + 6H_2O$. In order to make ohmic contact, In metal (99.99%) with 100 nm thickness was thermally evaporated onto the back side to n-type Si

Fig. 1 Synthesis of BDP-Sty



wafer, followed by annealing at 350°C for 30 s in nitrogen ambient. The BDP-Sty material was coated on the cleaned front surface of the n-Si by the spin coating at a spinning rate of 1000 rpm for 1 min in order to form a thin film. To form the rectifying contacts, Au metal was thermally evaporated onto the organic film through a metal shadow mask. The thickness of the interfacial layer was calculated to be about 128 nm from high-frequency measurement of the interface capacitance in the strong accumulation region.

3 Results and discussion

3.1 Theoretical studies

The synthesized BDP-Sty was first subjected to computational study based on DFT to computationally obtain the detail information about the electronic structure, conductivity and ground state optimize molecular geometry of the compound [39]. It has been known that Clausius–Mossotti equation, which establishes a relationship between its dielectric constant with polarizability and molar volume of any material is expressed by

$$\frac{\varepsilon_r - 1}{\varepsilon_r + 2} = \frac{4\pi N_A \alpha'}{3V_M} \quad (1)$$

where ε_r , V_M and N_A are dielectric constant, molar volume of material and Avogadro's constant, respectively, while α' is the polarizability volume in terms of $\alpha/4\pi\epsilon_0$ [40]. In this connection, the optimum structural geometry, Highest Occupied Molecular Orbital (HOMO) and Lowest Unoccupied Molecular Orbital (LUMO) analyses, MEP surface analysis, molecular static isotropic polarizability volume ($\alpha_{iso.} = \frac{1}{3}(\alpha_{xx} + \alpha_{yy} + \alpha_{zz})$) and molar volume of our compound were obtained by using Gaussian 09

program suite [39]. All computations were performed with DFT-B3LYP/6-311G(d,p) computational method by using keyword *tight* at the gas phase of isolated molecule [41, 42]. GaussView5 graphical interface program suite was used for visualization of the computed electronic structure properties [43]. The computed values of α_{xx} , α_{yy} and α_{zz} components of the polarizability were found as 728.4728 a_0^3 , 396.3244 a_0^3 and 174.3071 a_0^3 , respectively. Depending on these components, the molecular static isotropic polarizability volume, $\alpha_{iso.}$, was calculated as 433.0348 a_0^3 (or $6.4170 \times 10^{-23} \text{ cm}^3$) for the compound. The molar volume, V_M , was computed as 314.411 cm^3 . By using these computed values, the dielectric constant, ε_r was calculated as 3.94 with help of Clausius–Mossotti equation.

FMOs (frontier molecule orbitals), which are also called as LUMO and HOMO, use to investigate many molecular features such as ionization potential, polarizability, electron affinity, electronegativity, excitability, hardness, softness, basicity, acidity, global reactivity, electrical, electronic, charge transfers and electronic transitions of chemical systems [44–47]. The HOMO and LUMO drawings simulated of the compound at the gas phase with DFT-B3LYP/6-311G(d,p) computational level were depicted in Fig. 2a. Depending on these values, the computed results of aforementioned some molecular descriptors were listed in Table 1. For our compound, the LUMO, HOMO and energy band gap (ΔE) were theoretically found as -2.65 eV , -5.15 eV and 2.50 eV , respectively. As known from the literature, ΔE provides information about the conductivity of the compound. Since ΔE range for semiconductors is between 0.5 and 3.5 eV, BDP-Sty compound can have a semiconducting behavior [1, 48]. Moreover, it is well-known that the small value of the energy band gap between HOMO and LUMO indicate easily excitable, polarizable and chemically softness of

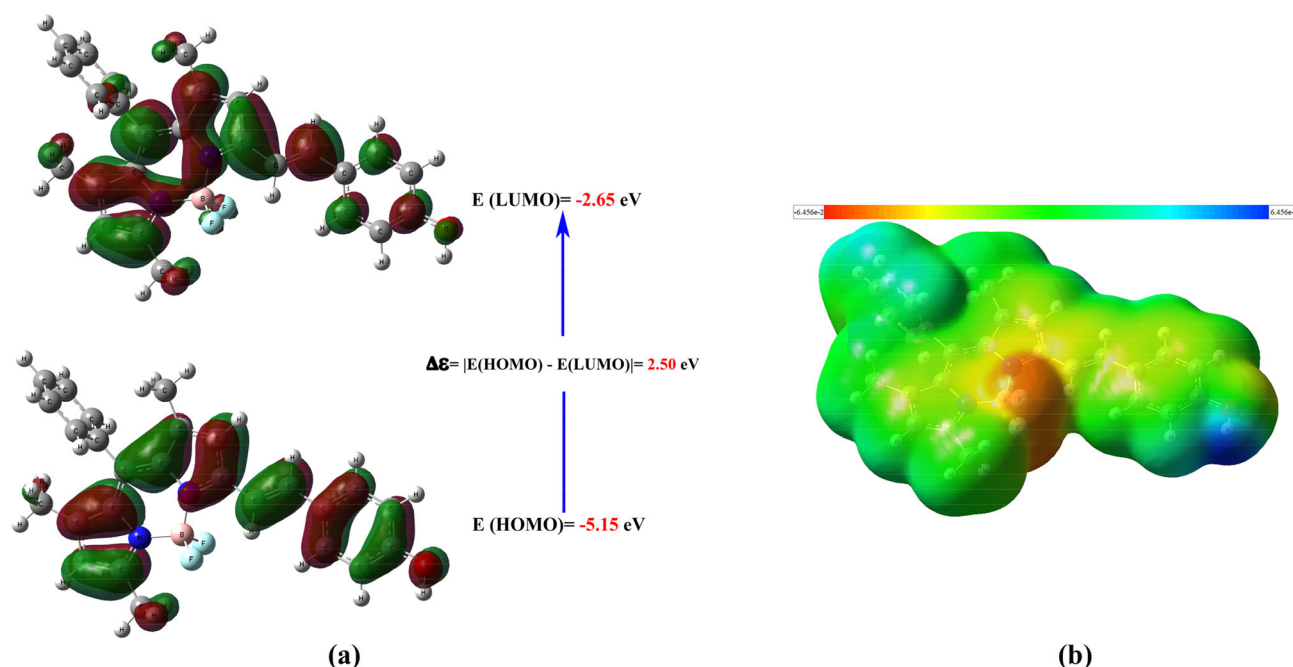


Fig. 2 a DFT computed energy levels of HOMO and LUMO b MEP surface map of the BDP-Sty compound

compound. Additionally, the easy excitability indicates that compound can have a good conductivity. The small energy band gap of 2.50 eV of our compound reveals a measure of its easily excitable, polarizable, chemically softness and good conductivity. Moreover, the electron affinity ($A = -E_{\text{LUMO}}$) and ionization potential ($I = -E_{\text{HOMO}}$) values for our compound were computed as 2.65 eV and 5.15 eV, respectively. As can be seen Fig. 1a, the HOMO is mostly placed over bonding pi molecular orbitals of BODIPY core group, olefin group and phenol ring,

Table 1 Computed some molecular descriptors depending on HOMO and LUMO energy values of the BDP-Sty

Parameters	Value (eV)
E_{LUMO}	- 2.65
E_{HOMO}	- 5.15
Energy band gap $ E_{\text{HOMO}} - E_{\text{LUMO}} $	2.50
Ionization potential ($I = -E_{\text{HOMO}}$)	5.15
Dielectric constant (ϵ_r)	3.94
Electron affinity ($A = -E_{\text{LUMO}}$)	2.65
Chemical hardness [$\eta = (I - A)/2$]	1.25
Chemical softness [$\eta = (I - A)/2$]	0.40
Electronegativity [$\chi = (I + A)/2$]	3.90
Chemical potential ($\mu = -(I + A)/2$)	- 3.90
Electrophilicity index ($\omega = \mu^2/2\eta$)	6.08
Maximum charge transfer index ($\Delta N_{\text{max.}} = -\mu/\eta$)	3.12

while the LUMO is mostly localized on anti-bonding pi molecular orbitals of BODIPY core group and olefin group. The lowest energy transition HOMO \rightarrow LUMO, which is the most likely transition in a compound, corresponds to $\pi \rightarrow \pi^*$ charge transfer in our compound. The electrophilic and nucleophilic reactive attack sites of the compound were investigated with molecular electrostatic potential (MEP) surface map. The MEP surface map of the compound was simulated with DFT-B3LYP/6-311G(d,p) computational level. The different colors on MEP surface map present different regions of electrostatic potential. Negatively-valued red and yellow places represent electrophilic reactive attack sites of electrostatic potential, whereas positively-valued blue places correspond to nucleophilic reactive attack sites of electrostatic potential. The regions with zero electrostatic potential are represented by green color. Figure 2b shows MEP surface map of the compound. The orange and blue colors around fluorine and phenol hydrogen atoms in our compound correspond to negative (electrophilic reactive attack sites) and positive (nucleophilic reactive attack site) electrostatic potential regions with values of -5.175 e^{-2} and $+6.456 \text{ e}^{-2}$, respectively. All these calculations clearly indicated that our synthesized BDP-Sty compound shows a semiconducting behavior, and its

possible use in heterojunction devices may be important for optoelectronic applications.

3.2 Illumination dependent I – V characteristics of Au/BDP-Sty/n-Si diode

Figure 3 shows the forward and reverse bias I – V characteristics of the Au/BDP-Sty/n-Si diode under dark and different illumination levels. The current value under illumination conditions in the reverse bias region was slightly higher than the current value in dark condition. The value of current in the reverse bias region increased with increasing light illumination, whereas there was small change in the forward current with the illumination. This indicates that the Au/BDP-Sty/n-Si diode shows a conventional photoconducting behavior. Also, as can be seen, the fabricated diode has a rectifier behavior. Therefore, the charge transport mechanism of the Au/BDP-Sty/n-Si diode obeys the thermionic emission (TE) theory, and the relation between the I , V and R_s is expressed as follows [3, 49]:

$$I = I_0 \left[\exp\left(\frac{q(V - IR_s)}{nkT}\right) - 1 \right] \quad (2)$$

where n , T , q , V and k are defined as ideality factor, temperature in Kelvin, electron charge, applied voltage and Boltzmann constant, respectively. I_0 defined as the saturation current is defined by the following equation:

$$I_0 = AA^*T^2 \exp\left[-\frac{q\Phi_b}{kT}\right] \quad (3)$$

where A and A^* are defined as effective diode area and Richardson coefficient ($112 \text{ A cm}^{-2} \text{ K}^{-2}$ for n-Si), respectively. Φ_b is the barrier height at zero bias and determined by the following equation:

$$\Phi_b = \frac{kT}{q} \ln\left(\frac{AA^*T^2}{I_0}\right) \quad (4)$$

Ideality factor (n) which clarifies the departure of the current transport mechanism from the ideal TE model is defined as

$$n = \frac{q}{kT} \frac{dV}{d(\ln I)} \quad (5)$$

The regions selected for the calculations were defined as $0.18 < V < 0.70 \text{ V}$ for dark and $0.20 < V < 0.75 \text{ V}$ for illumination levels. The values of n , Φ_b and I_0 calculated from the forward bias I – V characteristics for dark and different illumination conditions were given in Table 2. The n and Φ_b values were found to be 2.32 and 0.828 eV in dark, respectively. As seen, the n values of the diode were higher than 1 which indicates the diode shows non-ideal diode behavior due to the interface states, barrier inhomogeneity, surface states/traps and series resistance. The n values decreased with increasing illumination level which can be attributed to the increasing photo generated charge carriers under illumination in the interface of the device [1, 2, 18]. The values of Φ_b slightly increased with increasing illumination level due to the increasing charge carriers. Additionally, in Fig. 3, the intersection behavior of I – V curves was seen which seems to be an anomaly compared to the traditional behavior of ideal Schottky diodes. This behavior is attributed to the lack of free charge under low illumination level and then photo-current becomes increase as rapidly and hence leads an intersection at about a constant voltage point [16]. In this point, the value of current becomes almost independent from the illumination. Moreover, it can be seen in Fig. 3 that there was a fluctuation in the reverse bias I – V plots under illumination conditions which can be attributed to the high electron–hole separation efficacy of the strong internal and external electric fields which are in the same direction in the reverse bias.

In Schottky structures, another main parameter that effects the performance of the diode is series

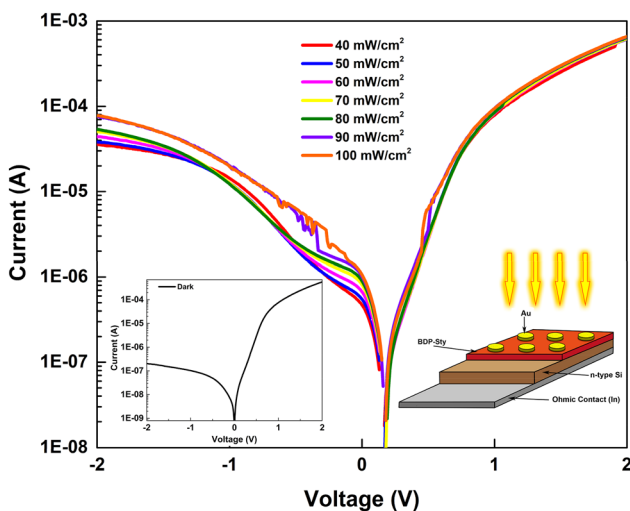


Fig. 3 I – V characteristics of the prepared diode. Inset shows the schematic representation of the fabricated diode

Table 2 The calculated ideality factor (n), reverse saturation current (I_0), barrier height (Φ_b) and series resistance (R_s) in dark and under different illumination levels

Illumination intensity (mW/cm ²)	n	I_0 (nA)	Φ_b (eV)	$dV/d(\ln I) - I$		$H(I) - I$	
				R_s (k Ω)	n	R_s (k Ω)	Φ_b (eV)
0	2.32	4.07	0.828	4.95	2.21	4.59	0.880
40	2.23	2.64	0.839	3.19	2.94	2.85	0.827
50	2.18	2.30	0.842	3.09	2.90	2.77	0.829
60	2.08	1.74	0.850	2.91	3.08	2.48	0.820
70	1.96	1.40	0.855	2.89	3.04	2.56	0.822
80	1.84	1.03	0.863	2.76	3.12	2.47	0.817
90	1.79	1.58	0.852	2.65	3.80	2.46	0.769
100	1.59	0.704	0.873	1.80	4.57	1.61	0.746

resistance (R_s). Cheung’s method was used to obtain the R_s values of Au/BDP-Sty/n-Si diode for dark and various illumination levels. Cheung’s functions model which defined a relation between R_s , I and V is expressed as [50]:

$$H(I) = V - n \frac{kT}{q} \ln \left(\frac{I}{AA^*T^2} \right) \tag{6}$$

$$H(I) = n\Phi_b + IR_s \tag{7}$$

$$\frac{dV}{d(\ln I)} = \frac{nkT}{q} + IR_s \tag{8}$$

A plot of $dV/d(\ln I)$ vs. I and $H(I)$ vs. I for prepared diode were drawn in Fig. 4a and b, respectively. Equations 7 and 8 show that, the slopes of the both plot of $H(I) - I$ and $dV/d(\ln I) - I$ give R_s of the Au/BDP-Sty/n-Si diode. The R_s , n and Φ_b values obtained from Cheung’s functions were listed in Table 2. As seen, the values of R_s obtained from Eqs. 7 and 8 are in agreement with each other. The decreasing R_s values with the increasing illumination level can be explained by the increasing of the free charge carrier concentration.

The conduction mechanisms of the prepared diode were analyzed by using the $\ln(I_F)$ vs $\ln(V_F)$ and $\ln(I_R)$ vs $V_R^{1/2}$ characteristics of the Au/BDP-Sty/n-Si diode. As seen in Fig. 5a, the prepared diode has four different linear part in different regions that shows power law behavior of $I \propto V^m$, where m is the constant and obtained from the slope of the $\ln(I) - \ln(V)$ plot. In the region I, the slope was found to be close to 1, which means that the current and voltage is nearly proportional, and the conduction mechanism shows the ohmic behavior. The slope of the region II was much higher than unity, and so TCLC can dominate in current mechanism. In addition, the m value of region III and IV was found to be about 5.34 and 3.05,

respectively, and the current mechanism can be explained by the SCLC [3, 49, 51]. Schottky emission (SE) and Poole–Frenkel emission (PFE) theories were used to study the current conduction mechanism of Au/BDP-Sty/n-Si diode in reverse bias [52]. The SE and PFE theory can be explained as:

$$I_R = AA^*T^2 \exp \left(\frac{\beta_{SC} V^{1/2}}{kTd^{1/2}} \right) \tag{9a}$$

$$I_R = I_0 \exp \left(\frac{\beta_{PF} V^{1/2}}{kTd^{1/2}} \right) \tag{9b}$$

where β_{SC} and β_{PF} are the Schottky and Poole–Frenkel field lowering coefficients, respectively. The theoretical values of β_{SC} and β_{PF} coefficients can be expressed as:

$$2\beta_{SC} = \beta_{PF} = \left(\frac{q^3}{\epsilon_r \epsilon_0 \pi} \right)^{1/2} \tag{10}$$

where ϵ_r is the permittivity of the interfacial layer. The theoretical values of β_{PF} and β_{SC} were calculated as 7.64×10^{-5} and 3.82×10^{-5} eV $m^{1/2} V^{-1/2}$, respectively. The experimentally calculated β values obtained from the slope of Fig. 5b were found to be 1.77×10^{-4} and 3.51×10^{-4} eV $m^{1/2} V^{-1/2}$ for dark and under 100 mW/cm² illumination level, respectively. These obtained results indicated that the obtained experimental β values are close to the theoretical β_{SC} coefficient, and so SE effect is more dominant in reverse direction [52].

It is known that interface states which are located between interfacial layer and semiconductor interface can control some electrical properties of SDs such as ideality factor and barrier height derived from $\ln(I) - V$ plots of the device. When the interface states in equilibrium with the semiconductor, the relation between density of interface states and

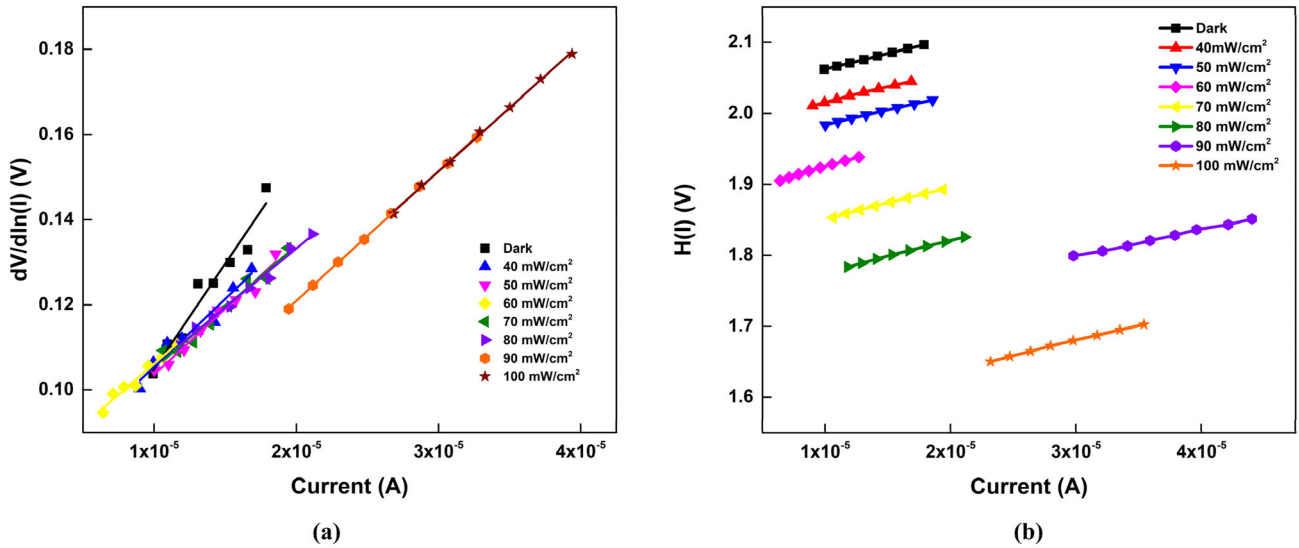


Fig. 4 a $dV/d(\ln I)$ vs. I and b $H(I)$ vs. I curves for the Au/BDP-Sty/n-Si diode under dark and illumination conditions

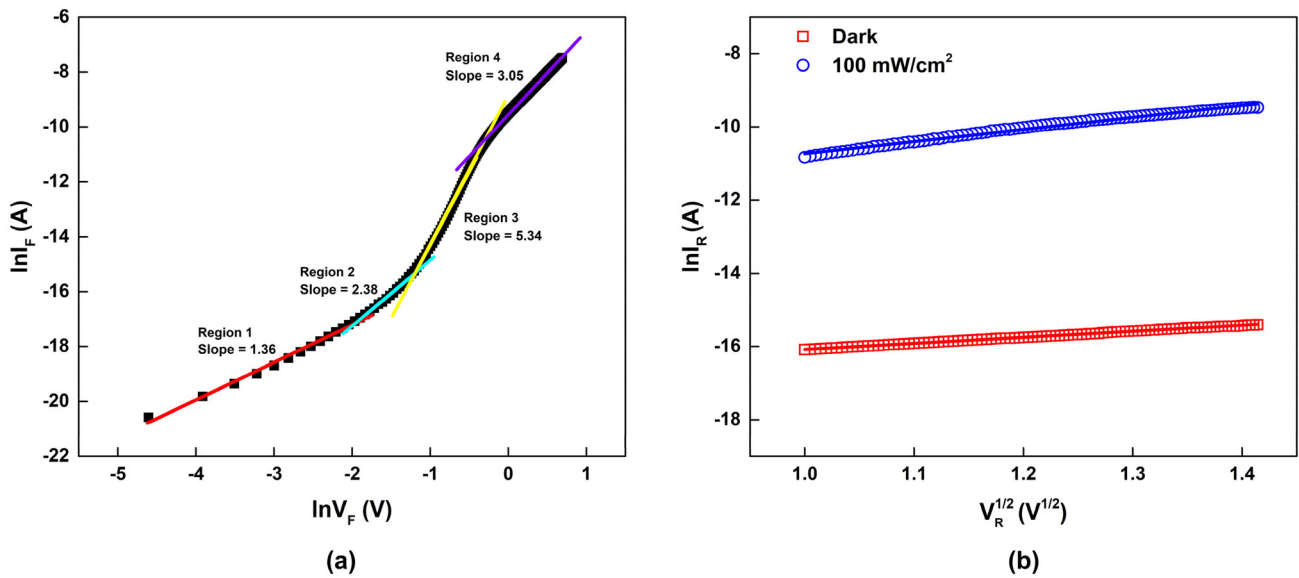


Fig. 5 a $\ln(I_F)$ vs. $\ln(V_F)$ and b $\ln(I_R)$ vs. $V_R^{1/2}$ curves for the Au/BDP-Sty/n-Si diode

ideality factor for n-type Schottky diode is defined by Card and Rhoderick as [51]:

$$N_{ss}(V) = \frac{1}{q} \left[\frac{\epsilon_i}{\delta_i} (n(V) - 1) - \frac{\epsilon_s}{W_D} \right] \tag{11}$$

where δ_i , W_D , ϵ_s and ϵ_i are the thickness of interface layer, space charge layer width (7.354×10^{-5} cm), dielectric constant of semiconductor and dielectric constant of interface, respectively. In n-type semiconductor, the energy of interface states is defined as:

$$E_c - E_{ss} = q(\Phi_e - V);$$

$$\Phi_e = \Phi_b + \beta V = \Phi_b + \left(1 - \frac{1}{n(V)}\right)V \tag{12}$$

where Φ_e and q are the effective barrier height and the electron charge, respectively.

Figure 6 shows the N_{ss} profiles of the Au/BDP-Sty/n-Si diode derived from the forward bias $I-V$ characteristics for dark and under different illumination intensity. The N_{ss} values of Au/BDP-Sty/n-Si diode is in the range of $7.15 \times 10^{11} \text{ eV}^{-1}\text{cm}^{-2}$ to $1.83 \times 10^{11} \text{ eV}^{-1}\text{cm}^{-2}$ under conditions of dark and $5.95 \times 10^{11} \text{ eV}^{-1}\text{cm}^{-2}$ to $1.08 \times 10^{11} \text{ eV}^{-1}\text{cm}^{-2}$ under

100 mW/cm². Figure 6 reveals a decrease in the N_{ss} with increasing illumination intensities which can be attributed to the discharge and charge of interface states under the effect of illumination [53, 54].

To understand the photovoltaic performance of diode, the forward current density–voltage (J – V) characteristics of illuminated Au/BDP-Sty/n-Si diode were analyzed (Fig. 7). The basic photovoltaic parameters of the diode are listed in Table 3 for various illumination conditions. As can be seen, while the V_{oc} value varies slightly with illumination, the J_{sc} value increases with increasing illumination intensity. This behavior can be attributed to the increasing in charge carrier concentration due to incident light absorption. Additionally, while increasing light intensity increases maximum electrical power ($P_{max} = J_{max} \times V_{max}$), fill factor ($FF = V_{max} \times J_{max} / V_{oc} \times J_{sc}$) slightly decreases from 26.26 to 20.62 with the light intensity.

In addition, it was observed that the photosensitivity ($S = I_{photo} / I_{dark}$) values under -2 V increased with the light intensity which shows that the Au/BDP-Sty/n-Si diode is sensitive to illumination intensities. In addition, it was observed that the photosensitivity ($S = I_{photo} / I_{dark}$) values under -2 V increased with the light intensity which shows that the Au/BDP-Sty/n-Si diode is sensitive to illumination intensities.

Short circuit current density, J_{sc} shows a linear change with illumination intensities, as seen in Table 3, and is in good agreement with the theory

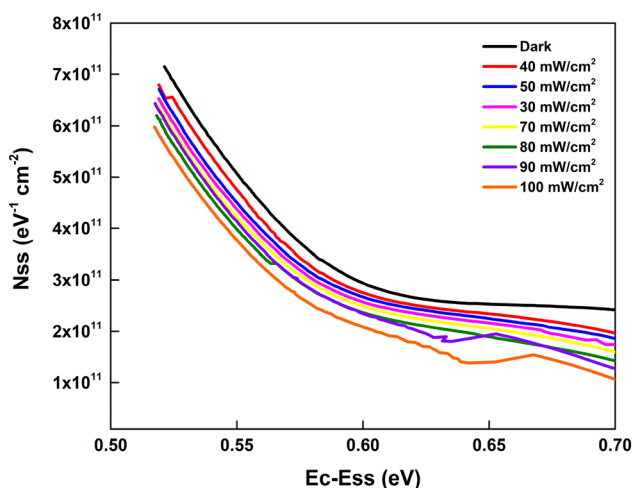


Fig. 6 Variation of N_{ss} with $E_c - E_{ss}$ for the Au/BDP-Sty/n-Si diode

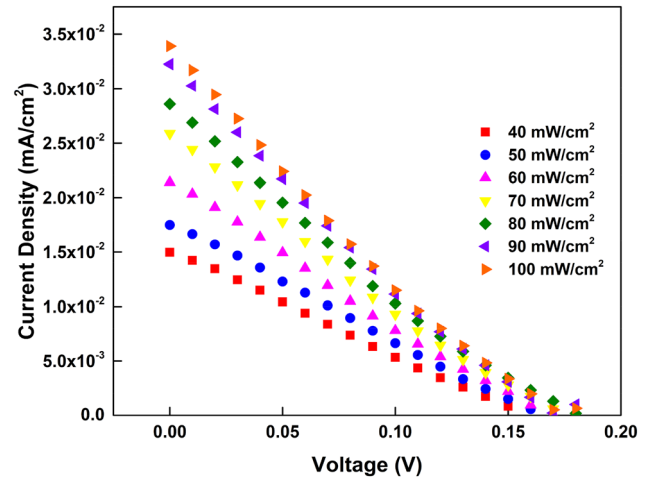


Fig. 7 J – V plots for the Au/BDP-Sty/n-Si diode

that can explain the relation between photocurrent and light intensity as

$$I_{photo} = \gamma P^\beta \tag{13}$$

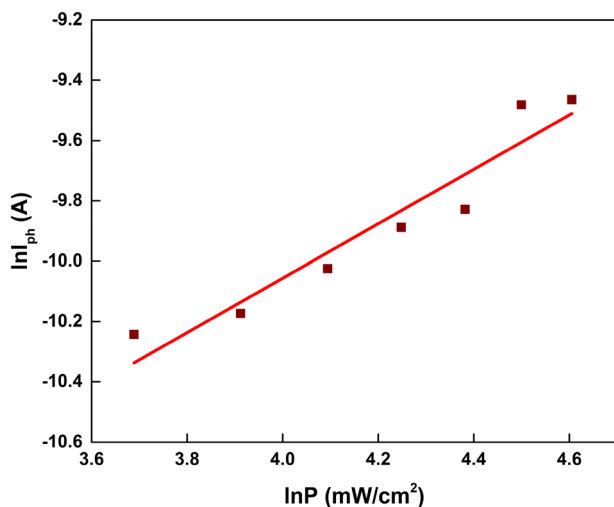
where γ is a constant, and β is an exponent, which depends on the process of the recombination such as monomolecular and bimolecular. As seen in Fig. 8, plot of $\ln(I_{ph})$ vs. $\ln(P)$ gives a linear relationship, and the value of β can be obtained from its slope. The β value for Au/BDP-Sty/n-Si/In diode was found to be 0.27, and this shows that photoconduction mechanism might be controlled by bimolecular recombination mechanism [55, 56].

4 Conclusion

In the presented work, we showed the synthesis of a α -styryl substituted BODIPY compound (BDP-Sty) was demonstrated its use as a semiconductor material in the fabrication of an Au/BDP-Sty/n-Si/In diode. Theoretical studies were performed with DFT theory analysis to investigate various molecular descriptors such as optimize ground state structure of the isolated compound, HOMO and LUMO simulations, and various molecular descriptors such as dielectric constant, electronegativity, chemical potential, and electrophilicity index. The electrical and photo response characteristics of the fabricated diode have been investigated for different illumination intensities. The I – V measurements revealed that the fabricated diode exhibited a good rectification behavior in dark. The main diode parameters such as I_0 , Φ_b , R_s , V_{oc} , J_{sc} and S were obtained as strong

Table 3 Photovoltaic parameters of the Au/BDP-Sty/n-Si device under various illumination levels

Power (mW/cm ²)	V_{oc} (V)	J_{sc} (mA/cm ²)	V_{max} (V)	I_{max} (μ A)	FF	P_{max} (W) $\times 10^{-4}$	S (at $V_R = -2$ V)
40	0.15	0.015	0.08	7.3	26.26	5.89	173.9
50	0.16	0.017	0.08	8.9	25.60	7.17	186.6
60	0.17	0.021	0.08	10.4	23.08	8.40	216.7
70	0.17	0.025	0.07	14.3	22.77	10.02	248.5
80	0.18	0.028	0.08	13.9	21.74	11.19	263.9
90	0.18	0.032	0.08	15.3	21.22	12.32	373.9
100	0.18	0.033	0.08	15.7	20.62	12.58	380.1

**Fig. 8** $\ln(I_{ph})$ vs $\ln(P)$ plot for the Au/BDP-Sty/n-Si diode

function of the illumination intensity. For instance, while the value of n is decreased from 2.32 to 1.59 with increasing illumination condition from dark to 100 mW/cm², the Φ_b values increased from 0.828 to 0.873 eV. Moreover, R_s values for dark calculated from $dV/d\ln(I)$ plot and Cheung's $H(I)$ function were found as 4.95 k Ω and 4.59 k Ω , respectively. The analysis of $\ln(I_F) - \ln(V_F)$ characteristics indicated that conduction mechanism is ohmic at low voltage and SCLC and TCLC conduction was dominated at higher voltage. It was also found that the conduction of the diode is dominated by the Schottky emission effect under reverse bias.

Declarations

Conflict of interest The authors declare that they have no known competing financial interests or personal relationships that could have appeared to influence the work reported in this paper.

References

1. W. Brütting, *Physics of Organic Semiconductors* (Wiley-VCH, Weinheim, 2005).
2. S.S. Li, *Semiconductor Physical Electronics*, 2nd edn. (Springer-Verlag, New York, 2006).
3. S.M. Sze, K.K. Ng, *Physics of Semiconductor Devices* (Wiley-Interscience, Hoboken, 2007).
4. A.A.M. Farag, I.S. Yahia, *Synth. Met.* **161**, 32 (2011)
5. S. Karadeniz, B. Baris, O.F. Yüksel, N. Tuğluoğlu, *Synth. Met.* **168**, 16 (2013)
6. O.F. Yüksel, N. Tuğluoğlu, H. Safak, Z. Nalçacıgil, M. Kuş, S. Karadeniz, *Thin Solid Films* **534**, 614 (2013)
7. F.A. Mir, S.U. Rehman, K. Asokan, S.H. Khan, G.M. Bhat, *J. Mater. Sci.: Mater. Electron.* **25**, 1258 (2014)
8. M. Yıldırım, A. Erdoğan, Ö.F. Yüksel, M. Kuş, M. Can et al., *J. Mater. Sci.: Mater. Electron.* **30**, 10408 (2019)
9. S. Demirezen, A. Eroğlu, Y. Azizian-Kalandaragh, Ş. Altındal, *J. Mater. Sci.: Mater. Electron.* **31**, 15589 (2020)
10. H.H. Gullu, D.E. Yildiz, L. Toppare, A. Çırpan, *J. Mater. Sci.: Mater. Electron.* **31**, 18816 (2020)
11. A.G. Imer, E. Kaya, A. Dere, A.G. Al-Sehemi, A.A. Al-Ghamdi et al., *J. Mater. Sci.: Mater. Electron.* **31**, 14665 (2020)
12. C. Wang, X. Zhang, W. Hu, *Chem. Soc. Rev.* **49**, 653 (2020)
13. P.R.S. Reddy, V. Janardhanam, K.H. Shim, S.N. Lee, A.A. Kumar et al., *Thin Solid Films* **713**, 8 (2020)
14. V.R. Reddy, C.V. Prasad, K.R. Reddy, *Solid State Sci.* **97**, 7 (2019)
15. S. Demirezen, H.G. Çetinkaya, M. Kara, F. Yakuphanoglu, Ş. Altındal, *Sens. Actuators A* **317**, 112449 (2021)
16. E. Arslan, Y. Badali, Ş. Altındal, E. Özbay, *J. Mater. Sci.: Mater. Electron.* **31**, 13167 (2020)
17. G. Ersöz, I. Yücedağ, S. Bayrakdar, Ş. Altındal, A. Gümüş, *J. Mater. Sci.: Mater. Electron.* **28**, 6413 (2017)
18. W. Hu, F. Bai, X. Gong, X. Zhan, H. Fu, T. Bjornholm, *Organic Optoelectronics* (Wiley-VCH, Weinheim, 2013).

19. F.M. Jin, Z.S. Su, B. Chu, P.F. Cheng, J.B. Wang et al., *Sci. Rep.* (2016). <https://doi.org/10.1038/srep26262>
20. K. Hunger, *Industrial Dyes: Chemistry, Properties, Applications* (Wiley-VCH, Weinheim, 2002).
21. T.D. Kim, K.S. Lee, *Macromol. Rapid Commun.* **36**, 943 (2015)
22. J.-F. Morin, *J. Mater. Chem. C* **5**, 12298 (2017)
23. S.A.A. Shah, M.H. Sayyad, N. Nasr, R.A. Toor, S. Sajjad et al., *J. Mater. Sci.: Mater. Electron.* **28**, 6552 (2017)
24. M. Yılmaz, A. Koçyiğit, Ş. Aydoğan, U. İncekara, A. Turşucu, H. Kaçus, *J. Mater. Sci.: Mater. Electron.* **31**, 21548 (2020)
25. A. Loudet, K. Burgess, *Chem. Rev.* **107**, 4891 (2007)
26. J.J. Chen, S.M. Conron, P. Erwin, M. Dimitriou, K. McAlahney, M.E. Thompson, *ACS Appl. Mater. Interfaces* **7**, 662 (2015)
27. D. Ho, R. Ozdemir, H. Kim, T. Earmme, H. Usta, C. Kim, *ChemPlusChem* **84**, 18 (2019)
28. M. Poddar, R. Misra, *Coord. Chem. Rev.* **421**, 22 (2020)
29. Y.Q. Fan, J.J. Zhang, Z.Y. Hong, H.Y. Qiu, Y. Li, S.C. Yin, *Polymers* **13**, 30 (2021)
30. S.P. Singh, T. Gayathri, *Eur. J. Org. Chem.* **2014**, 4689 (2014)
31. L. Bucher, N. Desbois, P.D. Harvey, G.D. Sharma, C.P. Gros, *Sol. RRL.* **1**, 1700127 (2017)
32. B.M. Squeo, V.G. Gregoriou, A. Avgeropoulos, S. Baysec, S. Allard et al., *Prog. Polym. Sci.* **71**, 26 (2017)
33. E. Özcan, B. Topaloğlu Aksoy, E. Tanrıverdi Eçik, A. Dere, A. Karabulut et al., *Inorg. Chem. Front.* **7**, 2920 (2020)
34. B. Topaloğlu Aksoy, G. Keşan, E. Özcan, E. Tanrıverdi Eçik, A. Dere et al., *New J. Chem.* **44**, 2155 (2020)
35. M. Özdemir, D. Choi, G. Kwon, Y. Zorlu, B. Coşut et al., *ACS Appl. Mater. Interfaces* **8**, 14077 (2016)
36. A. Tataroğlu, A.G. Al-Sehemi, M. Özdemir, R. Özdemir, H. Usta et al., *Physica B* **519**, 53 (2017)
37. T. Kilicoglu, Y.S. Ocak, *Microelectron. Eng.* **88**, 150 (2011)
38. F. Ali, A.H. Anila, N. Taye, R.G. Gonnade, S. Chattopadhyay, A. Das, *Chem. Commun.* **51**, 16932 (2015)
39. M.J. Frisch, G.W. Trucks, H.B. Schlegel, G.E. Scuseria, M.A. Robb et al., *Gaussian 09, Revision C.01* (Gaussian Inc, Wallingford, 2009).
40. Z. Tang, C.F. Chang, F. Bao, L. Tian, H.C. Liu et al., *Polymers* **13**, 284 (2021)
41. C.T. Lee, W.T. Yang, R.G. Parr, *Phys. Rev. B* **37**, 785 (1988)
42. A.D. Becke, *J. Chem. Phys.* **98**, 5648 (1993)
43. R. Dennington, T. Keith, J. Millam, *GaussView, Version 5* (Semicem Inc, Shawnee Mission, 2009).
44. K. Fukui, *Science* **218**, 747 (1982)
45. R.G. Pearson, *J. Org. Chem.* **54**, 1423 (1989)
46. P. Geerlings, F. De Proft, W. Langenaeker, *Chem. Rev.* **103**, 1793 (2003)
47. C.G. Zhan, J.A. Nichols, D.A. Dixon, *J. Phys. Chem. A* **107**, 4184 (2003)
48. P.W. Atkins, M.E. Hagerman, D.F. Shriver, *Inorganic Chemistry* (Oxford University Press, Oxford, 2010).
49. E.H. Rhoderick, R.H. Williams, *Metal-Semiconductor Contacts* (Clarendon Press, Oxford, 1988).
50. S.K. Cheung, N.W. Cheung, *Appl. Phys. Lett.* **49**, 85 (1986)
51. H.C. Card, E.H. Rhoderick, *J. Phys. D Appl. Phys.* **4**, 1589 (1971)
52. J.G. Simmons, *J. Phys. D Appl. Phys.* **4**, 613 (1971)
53. B. Akkal, Z. Benamara, N.B. Bouiadjra, S. Tizi, B. Gruzza, *Appl. Surf. Sci.* **253**, 1065 (2006)
54. O. Pakma, Ş. Çavdar, H. Koralay, N. Tuğluoğlu, Ö.F. Yüksel, *Physica B* **527**, 1 (2017)
55. E. Arene, J. Baixeras, *Phys. Rev. B* **30**, 2016 (1984)
56. A. Rose, *Concepts in Photoconductivity and Allied Problems* (Krieger Publishing Co, Huntington, 1978).

Publisher's Note Springer Nature remains neutral with regard to jurisdictional claims in published maps and institutional affiliations.